EXP 1-6

Mitigation of installed jet noise using porous flap trailing edges

Abstract

Incremental innovation (https://ideascale.com/blog/incremental-innovation/) on established aircraft platforms is driven by installing increasingly larger jet engines under the wing (Figure 1). Since the vertical distance to the ground is limited by the landing gear and the requirements for minimal ground clearance, larger engines are often installed closer to the wing. This causes additional acoustic installation penalties which can potentially neutralize any noise reduction benefits gained with the help of new engine technologies. One idea to reduce these additional acoustic installation penalties, i.e. modifying the flap trailing edge with porous material, is discussed in this article.

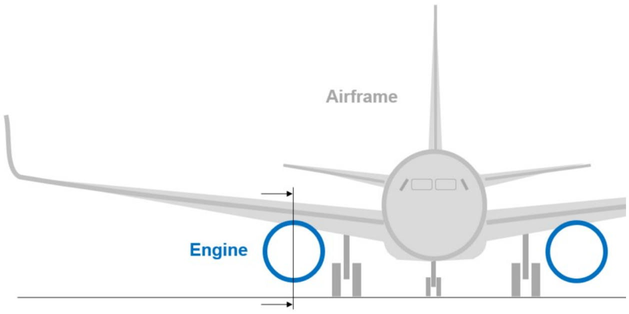

Figure 1: Engine integrated under the wing of a commercial airplane

The minimal installation noise is the noise of the isolated jet engine without the presence of the airframe. The **isolated jet noise** is in *this study* (Figure 2) determined for a single stream jet engine which issues a Ø50mm jet at a jet exit Mach number of 0.6. The test is a static test which means that the flight speed is zero.
The **installed jet noise** is determined by adding at least the wing to the installation. In the presented test, a generic two-element wing geometry is used. It consists of a main wing substitute and a 25° deflected flap. Both elements add up to a combined chord length of 150mm.
The relative positioning between wing and engine, i.e. the engine integration, is defined by the length L between the engine outlet plane and the flap trailing edge (horizontal proximity) as well as the height H between the engine axis and the flap trailing edge (vertical proximity).

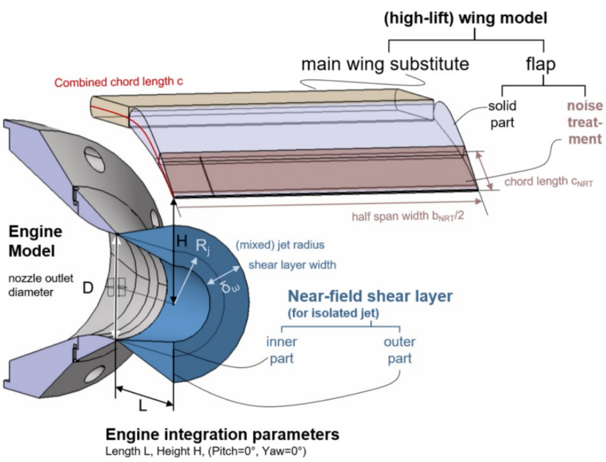

Figure 2: Scheme of the tested installed engine model

The acoustic installation effect (or, alternatively: installation penalty) is the arithmetic difference between the installed jet noise and isolated jet noise.
There are two installed test builds, which have different trailing edge inserts: The baseline configuration is completely solid, whereas the adapted configuration is equipped with a porous trailing edge.
The difference between the installed jet noise of the two configurations shows whether the noise reduction technology works and to which extent installation noise can be reduced.
All in all, this is an experimental study of acoustics with microphones and the flow with pitot tubes. The actual acoustic and flow data are given in files.

Contributed by: **Christian Jente, Henri Siller** — *DLR Deutsches Zentrum für Luft- und Raumfahrt*

Front Page | Introduction | Review of experimental studies | Description | Experimental Set Up | Measurement Quantities and Techniques | Data Quality and Accuracy | Measurement Data and Results

Deprecated: Creation of dynamic property GuzzleHttp\Handler\CurlMultiHandler::$_mh is deprecated in **/var/www/html/mediawiki-1.39.7/vendor/guzzlehttp/guzzle/src/Handler/CurlMultiHandler.php** on line **103**

EXP 1-6 Introduction

Mitigation of installed jet noise using porous flap trailing edges

Introduction

Isolated jet flow is characterized by its potential core and jet shear layer in the aerodynamic near field (or: initial merging zone - see Fig.3). Placing a wing in close vicinity to the flow creates a semi-confined flow problem which is somewhat related to the family of jet impingement problems. The wing provides an interaction surface of finite length which deforms the jet. Due to the wing's contour curvature and inclination, the flow is here minimally deflected towards the ground. Alternative experiments with plates show jet attachment due to the Coanda effect.

In acoustic terms, the installation of the jet engine to the wing and its flap generates excess noise due to the interaction of the body surface with unsteady flow fluctuations issued by the pressure wave of the jet wave packets (https://en.wikipedia.org/wiki/Wave_packet).

The two general acoustic installation mechanisms are:

- **Wavelengths shorter than the engine integration length L** are reflected on the pressure side (i.e. under the wing/on the shielded side) and directed towards the ground. This causes high-frequency excess noise under the wing compared to the isolated jet.
- **Wavelengths larger than the engine integration length L** (low frequency range) cannot be reflected. The unsteady fluctuations propagate towards the flap trailing edge where they become acoustically relevant and scatter as sound into the far-field. The sound intensity is proportional to the aerodynamic load, hence called loading noise.

Apart from these two standard effects, there is an additional effect, the jet-flap interaction effect, which is only relevant for close installations:

- The flap trailing edge is here installed at a position which would be otherwise claimed by the jet shear layer of the *isolated* jet (Figure 3). The conflict of interest is resolved by a deformation of the jet. Furthermore, the jet shear layer (as well as the potential core of the jet) support various types of modes which propagate either in upstream or downstream direction. They enable a feedback loop between the engine lip and the flap trailing edge. This creates significant broadband and tonal excess noise, especially for **wavelengths equal to the engine integration length**.

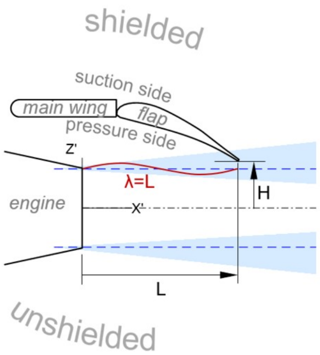

Figure 3: Engine integrated under the wing vs. near-field shear layer of the *isolated* jet

---

The purpose of this experimental study is to demonstrate and measure by microphones the overall noise reduction by using a partly porous flap, and also to evaluate the noise reduction effect by the three frequency ranges described above. The test hypothesis is that:

- The low-frequency loading noise effect can be reduced by allowing partial equalization of pressure fluctuations on the pressure side and suction side. This is possible since the porous material is permeable.
- Porous material may also reduce the mid-frequency jet-flap interaction effect by reducing coherence due to the irregular geometry of the trailing edge and thereby limiting the feedback mechanism.

The nomenclature (Table 1) is meant to support the readability ot this article:

Table 1: Nomenclature

abbreviation	explanation
AIAA	American Institute of Aeronautics and Astronautics
BL	solid baseline flap (w/o noise reduction technology)
BS	Braunschweig
DAQ	data acquisitioning unit
DJ	DJINN, *EU research project*, Grant agreement ID: 861438 (https://cordis.europa.eu/project/id/861438)
DLR	Deutsches Zentrum für Luft- und Raumfahrt e.V., i.e. the German Aerospace Center
ENG	centerpoint of engine (bypass) nozzle outlet, a measurement reference point
JExTRA	*a DLR test facility*, designed for jet noise experiments at AT-TRA
JFI	jet-flap interaction
NF	*here:* the aerodynamic near-field of the jet
NPR	nozzle pressure ratio
NRT	noise reduction technology
PA	porous aluminium
PSD	power spectral density
S/L	shear layer
SPL	sound pressure level
TDC	top dead center
TR	temperature ratio between jet and test room
w/o	without
w.r.t.	with respect to

Contributed by: **Christian Jente, Henri Siller** — *DLR Deutsches Zentrum für Luft- und Raumfahrt*

EXP 1-6 Review of Studies

Mitigation of installed jet noise using porous flap trailing edges

Review of Experimental Studies and choice of test case

- There is a number of published experiments which characterize aerodynamics and aeroacoustics of the isolated jet and the installed jet [1-9].
- There are also a few experiments on porous materials: The very porous aluminum PA80-110 trailing edge insert - which is featured in the present experiment - has been characterized for a cruise wing [10-12].
- **The present experiment does combine the installed jet with the PA80-110 noise reduction technology**, here adapted as a trailing edge insert in the flap, and is published in [13-15]. **The test case is based on** 15 (https://elib.dlr.de/186938/).
- It was conducted in the DLR JExTRA test facility in Berlin [16]. The facility has been cross-compared to other test facilities in Europe and America [17].
- Similar or even more complex cases towards the real aircraft including the flight effect were published in the mean time [18-21].

Qualitative comparison is possible w.r.t. installed jet noise test cases using porous inserts of other material and geometry. The purpose of this wiki entry and data exchange it to allow experimental cross-comparison as well as CFD/CAA validation.

---

1 **Bridges, J., and Wernet, M.**, " Establishing Consensus Turbulence Statistics for Hot Subsonic Jets," 16th AIAA/CEAS Aeroacoustics Conference, 2010. DOI 10.2514/6.2010-3751 (https://doi.org/10.2514/6.2010-3751) Manuscript (https://ntrs.nasa.gov/api/citations/20110016019/downloads/20110016019.pdf)
2 **Witze, P. O.**, "Centerline Velocity Decay of Compressible Free Jets", AIAA Journal, Vol. 12, No. 4, 1974, pp. 417–418. DOI 10.2514/3.49262 (https://doi.org/10.2514/3.49262)

3 **Viswanathan K.**, "Characteristics of jet noise: A synthesis". International Journal of Aeroacoustics. 2024;23(3-4):184-284. DOI 10.1177/1475472X241230653 (https://doi.org/10.1177/1475472X241230653)

---

4 **Lawrence, J.**, "Aeroacoustic interactions of installed subsonic round jets". PhD thesis, University of Southampton, 2014 SOTON EPrints ID: 367059 (http://eprints.soton.ac.uk/id/eprint/367059)
5 **Jente, C.**, "Strahl-Klappen-Interferenz - wie bedeutsam ist die Interaktionsschallquelle am Flugzeug", DAGA 2022 - 48. Jahrestagung für Akustik, Deutsche Gesellschaft für Akustik e.V. (DEGA), April 2022, pp. 1278-1281. Manuscript (https://elib.dlr.de/186298/)
6 **Cavalieri, A. V., Jordan, P., Wolf, W. R., and Gervais, Y.**, "Scattering of wavepackets by a flat plate in the vicinity of a turbulent jet", Journal of Sound and Vibration, Vol. 333, No. 24, 2014, pp. 6516-6531. DOI 10.1016/j.jsv.2014.07.029 (https://doi.org/10.1016/j.jsv.2014.07.029)
7 **Jordan, P., Jaunet, V., Towne, A., Cavalieri, A. V. G., Colonius, T., Schmidt, O., and Agarwal, A.**, "Jet-flap interaction tones", Journal of Fluid Mechanics, Vol. 853, 2018, pp. 333-358. DOI 10.1017/jfm.2018.566 (https://doi.org/10.1017/jfm.2018.566)
8 **Rego, L., Casalino, D., Avallone, F., and Ragni, D.**, "Noise Amplification Effects due to Jet-Surface Interaction", AIAA Scitech 2019 Forum, AIAA SciTech Forum, American Institute of Aeronautics and Astronautics, 2019. DOI 10.2514/6.2019-0001 (https://doi.org/10.2514/6.2019-0001) Manuscript (https://pure.tudelft.nl/ws/portalfiles/portal/52023812/6.2019_0001.pdf)
9 **Jente, C.**, "Jet-Flap Interaction Noise of Highly Integrated UHBR Turbofans". DLR-Forschungsbericht. DLR-FB-2024-19. Dissertation. Technische Universität Carolo-Wilhelmina Braunschweig. DOI 10.57676/1281-ze36. (https://doi.org/10.57676/1281-ze36)

---

10 **Herr, M., Rossignol, K.-S., Delfs, J., Lippitz, N., and Mößner, M.**, "Specification of Porous Materials for Low-Noise Trailing-Edge Applications", AIAA2014-3041. DOI 10.2514/6.2014-3041 (https://doi.org/10.2514/6.2014-3041) Manuscript (https://elib.dlr.de/91095/)
11 **Lippitz, N.**, "Poröse Materialien zur Reduzierung von Hinterkantenschall an Flugzeugflügeln", PhD thesis, Technische Universität Braunschweig, 2017.
12 **Schmidt, J.**, "Aeroakustische Untersuchungen an porösen Hinterkanten", Master's thesis, Technische Universität Braunschweig, 2019.

---

13 **Schmidt, J., and Jente, C.**, "Noise reduction of Jet-Flap-Interaction using porous trailing edges, perforated and slotted surfaces". 1st DJINN Conference, 2021, Online, Brussels/ Belgium. Presentation (https://elib.dlr.de/146675/)
14 **Jente, C**. "Porous flap trailing edges for the reduction of jet-flap interaction noise", ENODISE/DJINN/INVENTOR Public Workshop "Advanced Porous Treatment, liners and metamaterials for engine and airframe noise mitigation", 2022, Aachen, Germany. Presentation (https://elib.dlr.de/189783/)
15 **Jente, C. Schmidt, J. Delfs, J. Rossignol, K., Pott-Pollenske, M., and Siller, H.**, "Noise reduction potential of flow permeable materials for jet-flap interaction noise". 28th AIAA/CEAS Aeroacoustics Conference, 2022, Southampton, UK. DOI 10.2514/6.2022-3040 (https://doi.org/10.2514/6.2022-3040) Manuscript (https://elib.dlr.de/186938/).-------

16 **Siller, H., Nussbaumer, M., Hayat, W., Bassetti, A., Funke, S., Hage, W., and Meyer, R.**, "Ein kleiner Freistrahlprüfstand für aeroakustische Messungen", DAGA 2022 - 42. Jahrestagung für Akustik, Deutsche Gesellschaft für Akustik e.V. (DEGA), March 2016, pp. 363-366. DEGA link (https://pub.dega-akustik.de/DAGA_2016/data/articles/000348.pdf)
17 **Jente, C. und Siller, H. und Christophe, J., and Lawrence, J.**, "Isolated jet noise cross-comparison in various EU small and mid-size test facilities and geometric far-field". The DJINN-ENODISE conference: Aeroacoustic Installation Effects in Conventional and New Aircraft Propulsion Systems, 2023, Berlin, Germany. Presentation (https://elib.dlr.de/199634/)

---

18 **Jente, C., Huber, J., Renard, F., Goffredi, T., and Paladini, E.**, "Jet-flap installation noise of pylon mounted jet engine on 3D wing", 30th AIAA/CEAS Aeroacoustics Conference, 2024, Rome, Italy. DOI 10.2514/6.2024-3309 (https://doi.org/10.2514/6.2024-3309) Manuscript (https://elib.dlr.de/204661/).
19 **Jente, C. Huber, J., Ekoule, C., Goffredi, T. and Paladini, E.**, "Porous Flap Trailing Edges for the Reduction of Jet Installation Noise", pp. 1179-1182. DAGA 2024 (https://pub.dega-akustik.de/DAGA_2024), 50. Jahrestagung für Akustik, 2024, Hannover, Germany. ISBN 978-3-939296-22-5 Manuscript (https://elib.dlr.de/204078/)
20 **Rego, L., Ragni, D., Avallone, F., Casalino, D., Zamponi, R., and Schram, C.**, "Jet-installation noise reduction with flow-permeable materials", Journal of Sound and Vibration, Vol. 498, 2021, DOI 10.1016/j.jsv.2021.115959 (https://doi.org/10.1016/j.jsv.2021.115959)
21 **Sengupta, G.**, "Analysis of jet-airframe interaction noise", 8th Aeroacoustics Conference, AIAA, Atlanta, GA, USA, 1983. DOI 10.2514/6.1983-783 (https://doi.org/10.2514/6.1983-783)

Contributed by: **Christian Jente, Henri Siller** — *DLR Deutsches Zentrum für Luft- und Raumfahrt*

Front Page	Introduction	Review of experimental studies	Description	Experimental Set Up	Measurement Quantities and Techniques	Data Quality and Accuracy	Measurement Data and Results

EXP 1-6 Description

Mitigation of installed jet noise using porous flap trailing edges

Front Page	Introduction	Review of experimental studies	Description	Experimental Set Up	Measurement Quantities and Techniques	Data Quality and Accuracy	Measurement Data and Results

Description of Study Test Case

The engine is tested isolated (i.e. without wing) as well as installed under the wing (as shown in Figure 2 and Figure 3), both, with and without noise reduction technology (NRT).

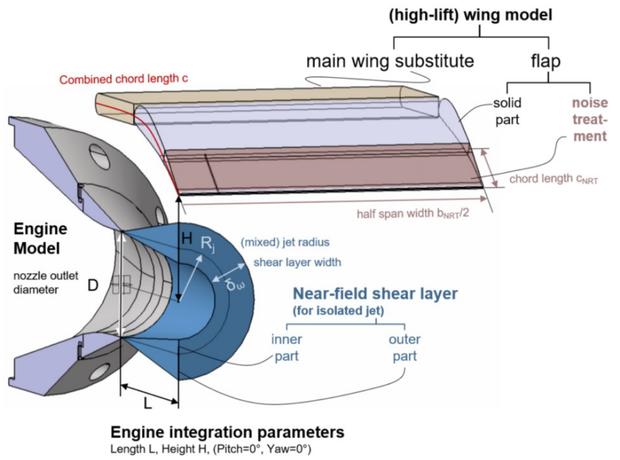

Figure 2: Scheme of installed engine

The geometrical parameters are given in Table 2.

Table 2: Test case parameters

Engine		
Nozzle outlet diameter	D	50mm
Jet diameter	R_j	25mm
Wing model		
Combined chord length	c	150mm
span width	b	254mm
flap deflection angle	δ_F	25°
porous chord length	c_{NRT}	254mm
porous span width	b_{NRT}	30mm
Engine Integration parameters		
Length	L	30mm
Height	H	100mm
Pitch	θ	0°
Yaw	ψ	0°

Engine model

The DJINN WP1 baseline nozzle DLR-DJ50 (depicted in Figure 4) is a single-stream round nozzle with an outlet diameter of Ø50mm. It has been designed by DLR-B (Alessandro Bassetti) and 3D-printed by DLR-B out of resin-like material using stereolithography. The model scale to a modern UHBR jet engine is approximately 1:40.

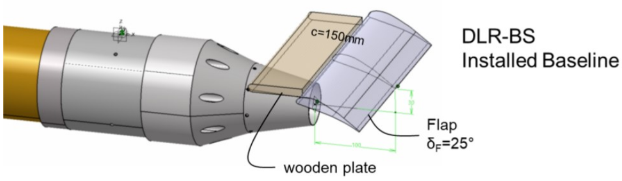

Figure 4: Installed engine

Wing model

The wing is approximated by a generic geometry which consists of a wooden main wing substitute and an adjacent flap (i.e. there is no gap). Both elements amount to a total chord length of c=150mm. The wing model is not inclined. The flap is deflected by 25°. Both the Baseline and the NRT flaps (Figure 5) have been investigated. The NRT flap trailing edge (last 30mm of chord length) can be exchanged by different noise reduction technologies.

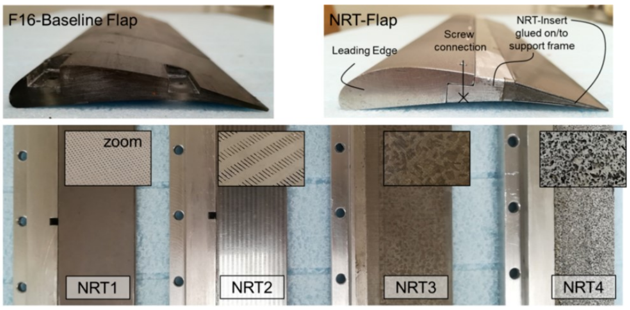

Figure 5: Baseline flap and NRT flaps. In the present study, only trailing edge option NRT4 was used.

Flap insert with noise reduction technology

The tested material is the porous aluminium PA80-110 (reference charge) and was referred to *NRT4* during the test [15]. The material was characterized by Technische Universität Braunschweig with a specific flow resistance (https://asastandards.org/terms/specific-flow-resistance/) of R=145.5±1.7 [10^3 Ns/m^4] a porosity of 46% [10,11] and a permeability of $4.3 \cdot 10^{-9}$ m^2.

Engine integration parameters

The engine integration parameters are displayed in Figures 2 and 3: The engine integration height is defined between engine axis and flap trailing edge as H=30mm. The engine integration length is defined engine outlet plane and flap trailing edge as L=100mm. Engine pitch and engine yaw are zero.

Engine operations

The engine is operated in static conditions at a jet Mach number of $M_j = 0.605$ and isothermal cold air conditions for $T_0 = T_j = 27°C$ close to standard atmospheric pressure of $p_0 = 101325 Pa$ (exact values are listed in the data files). The jet exit velocity is $U_j = 210 m/s$. The corresponding jet Reynolds number of $Re_D = 6.9 \cdot 10^5$ is greater than the critical Reynolds number of $5 \cdot 10^5$ which is needed to avoid a Reynolds number dependency due to small model size (https://doi.org/10.1177/1475472X241230653) [3]. Typical CFD-RANS Input Parameters are listed in Table 3.

Table 3: CFD-RANS Input Parameters

Physical Property	Definition	Value
Nozzle Pressure Ratio	$NPR := \frac{p_{t,j}}{p_0}$	1.2798
Static Temperature Ratio	$TR := \frac{T_j}{T_0}$	1 (isothermal)

Contributed by: **Christian Jente, Henri Siller** — *DLR Deutsches Zentrum für Luft- und Raumfahrt*

Deprecated: Creation of dynamic property GuzzleHttp\Handler\CurlMultiHandler::$_mh is deprecated in **/var/www/html/mediawiki-1.39.7/vendor/guzzlehttp/guzzle/src/Handler/CurlMultiHandler.php** on line **103**

EXP 1-6 Experimental Set Up

Mitigation of installed jet noise using porous flap trailing edges

Experimental Setup

The experiment was conducted at the **DLR-JExTRA facility**, a small scale jet test rig with an open test section. At the time of the test in July 2021, it was located at Müller-Breslau-Straße 8, 10623 Berlin-Charlottenburg/Germany and co-used by DLR (https://www.dlr.de/en)-Berlin and Technische Universität Berlin (https://www.tu.berlin/), Institut für Strömungsmechanik und Technische Akustik [1] (https://www.tu.berlin/ista). The test rig is installed in a test room (Figure 6) of dimension [Length x Width x Height] 11.5m x 5m x 2.5m.

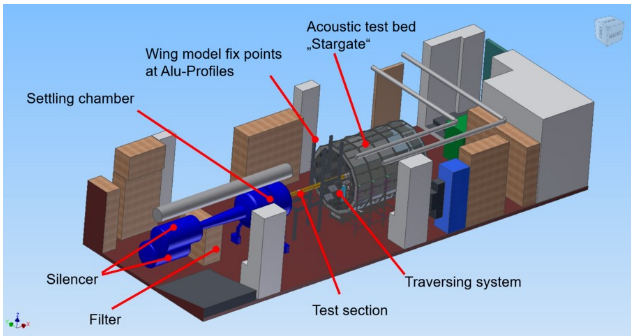

Figure 6: JExTRA test room K14

Air supply

JExTRA's **pressurized air supply** is a conventionally designed blow down rig. This means, motor and compressor are located in an adjacent room (Figure 7) and the supply duct is straight and fairly large compared to the tested nozzle: The settling chamber is of diameter Ø1000mm (area ratio 400) and the engine interface duct is a Ø100mm brass pipe (area ratio 4). The rig is designed to avoid internal rig noise: Direct placement of instrumentation, such as pitot probes, in the flow duct is avoided, with exception of the temperature probe which is well-placed in the low speed settling chamber (< 1m/s).
The powertrain contains an RPM-controlled (100-3000 RPM) HANSA (http://www.hansa-motoren.de/) motor type G18 (No. 649289, 440V, 164A, 65 kW), a gear box and a centrifugal compressor. The volumetric flow limit of the centrifugal compressor type DEMAG Sez 3F (No. 4902) is 2200 m³/h (standard atm. (https://en.wikipedia.org/wiki/International_Standard_Atmosphere), 0.73 kg/s). There is also a theoretical lower limit for the volumetric flow, since centrifugal compressor operations are unstable below the surge limit. To avoid running into the surge limit, higher volumetric flow than necessary is delivered and the excess air is discharged early via bypass pipes. The theoretical maximum pressure ratio at the compressor outlet is p_t/p_0 = 1.7. Assuming no pressure losses, this corresponds to a jet Mach number of M_j=0.9. The electrical components of the 2021 test rig version allow for safe testing until 2600 RPM which corresponds to M_j=0.76 for the tested nozzle.

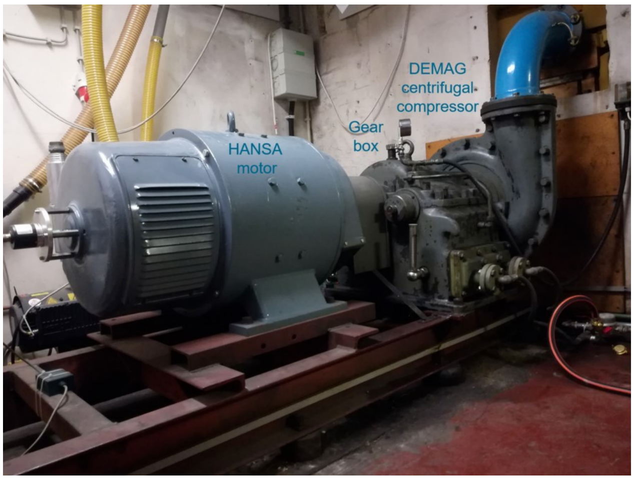

Figure 7: JExTRA power train in room K13

Model installation on rig

The model coordinate system (blue) is a right hand oriented system originating at the centerpoint of the nozzle outlet plane. X is the streamwise coordinate, Y is the coordinate in spanwise direction of the wing, and Z is the model's height coordinate. The polar angles will be measured aft-to-front (engine supplier coordinates), and not front-to-aft (airframe industry coordinates). The model is installed sideways in the test facility: the model top position is depicted by the triangular arrow in Figure 8.

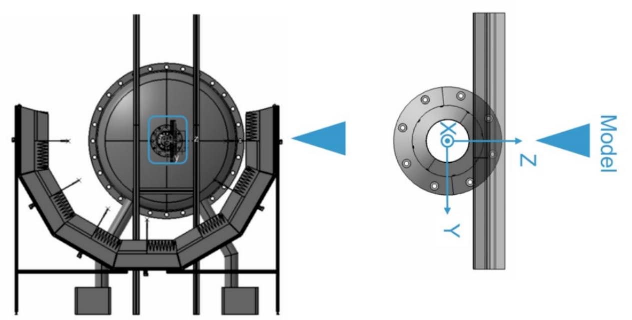

Figure 8: Rotated model vs JExTRA coordinates

The engine model is mounted at the JExTRA facility interface (Figure 9) using an existing engine adapter.

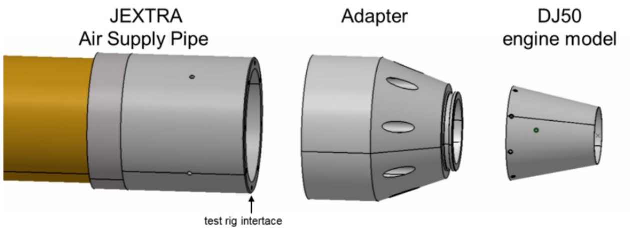

Figure 9: Engine interface

The wing model is held by a modular profile system (ITEM (https://de.wikipedia.org/wiki/Item_Industrietechnik)). The flap is embedded in a form-fit holder (Figure 10) (design: Johannes Schmidt) which enables high-speed testing. Moreover, the flap deflection angle, the engine integration height and engine integration length can be adjusted with the same device.

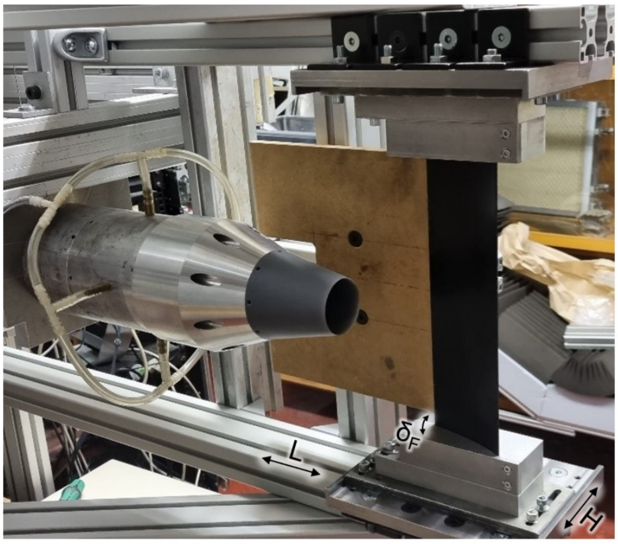

Figure 10: Adjustment of flap deflection angle, engine integration height and engine integration length.

Acoustic test

The acoustic test bed (Figure 11) [2] (https://pub.dega-akustik.de/DAGA_2016/data/articles/000348.pdf) is shaped like a cylinder (or more precise: an extruded dodecagon) which was nicknamed “Stargate” for its shape and appearance (Design: Alessandro Bassetti).

The installation space is approximately [Length x Width x Height] 2.5m x 2m x 2.5m.

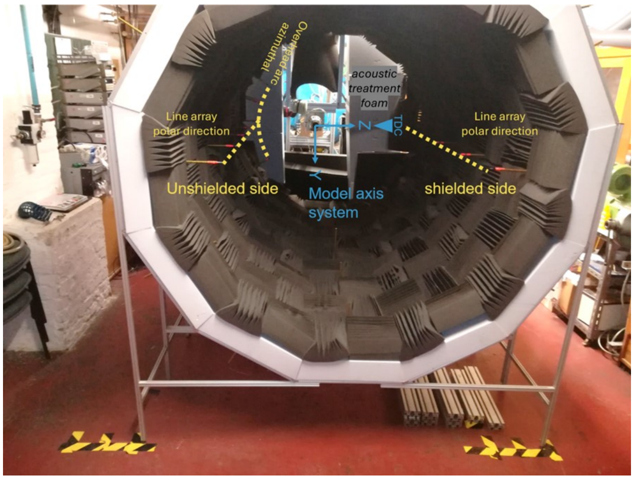

Figure 11: Microphone Setup for Acoustic test. The image has been taken during the isolated jet engine sub-test. View from a downstream position towards the nozzle exit.

The acoustical relevant space is of size [Radius x Length] 0.72m x 2.45m, which corresponds to a volume of ~4 m³. The foam depth is characterized by R=120mm full material (to wall) and R=80mm serrated foam.

- Base Layer (white): 100mm full material
- Top layer (dark gray): 20mm full material, [Height x base side] 80mm x 24.25mm serrated foam

The upstream side of the Stargate was mostly closed with foam plates for acoustic reasons. In close vicinity of the supply pipe it has been left open in order to avoid interfering with any jet entrainment physics. The downstream side of the Stargate is left open. The wall approx. at x=4m downstream the engine exit is treated with foam.

Steady aerodynamic test

Steady aerodynamic data is gathered with help of a measurement rake. The rake is mounted on a traversing unit (Figure 12) borrowed from the hot wire measurement system (of Robert Meyer). The lines emanating from the rake are pitot tubes. A positioning device (Figure 13) was used to adjust rake and model coordinates.

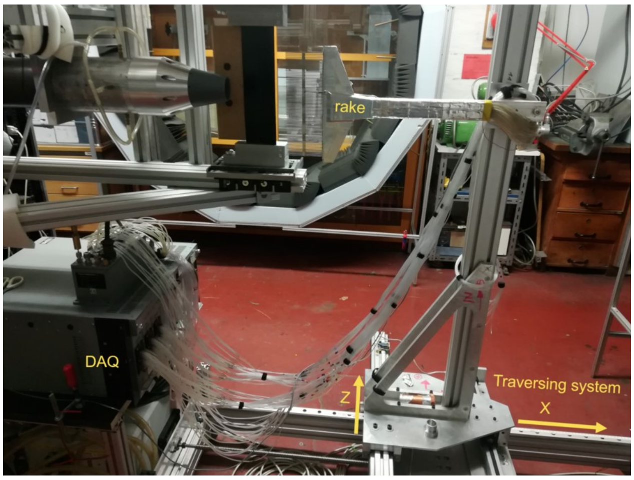

Figure 12: Rake setup on traversing system for steady aerodynamics tests

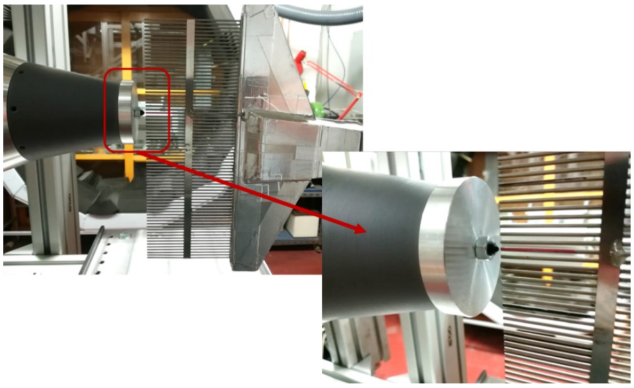
Figure 13: Initial setup of the rake, by blocking the nozzle exit with a cylindrical lid and centering with a headless screw.

Contributed by: **Christian Jente, Henri Siller** — *DLR - Deutsches Zentrum für Luft- und Raumfahrt*

Front Page | Introduction | Review of experimental studies | Description | Experimental Set Up | Measurement Quantities and Techniques | Data Quality and Accuracy | Measurement Data and Results

This page was last edited on 15 October 2025, at 15:19.

EXP 1-6 Measurement Quantities and Techniques

Mitigation of installed jet noise using porous flap trailing edges

Front Page | Introduction | Review of experimental studies | Description | Experimental Set Up | Measurement Quantities and Techniques | Data Quality and Accuracy | Measurement Data and Results

Measurement quantities and techniques

Acoustic test

The acoustic setup (Figure 11) contains 13 microphones, which can be divided into the following three groups:

- Polar / flyover line:
  - 6x unshielded side
  - 4x shielded side
- Azimuthal / overhead arc:
  - 4x on shielded side

The microphones are located at the end of the metal rods (orange tapes in Figure 11 indicate the microphone positions). The exact coordinates are listed in the data files.

The predominantly used microphone type is Microtech Gefell (https://www.microtechgefell.de/) MK301 (https://www.microtechgefell.de/mikrofonkapsel?wl=469-MK301) is a condenser microphone (https://en.wikipedia.org/wiki/Microphone#Condenser) which records sound pressure (https://en.wikipedia.org/wiki/Sound_pressure) over time, i.e. the difference between the local and the ambient pressure.

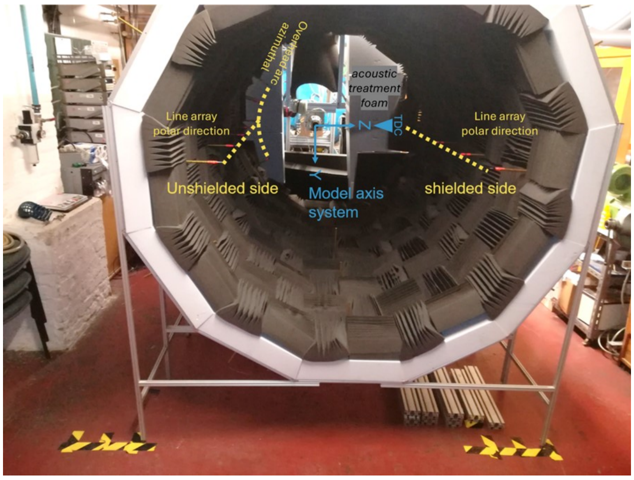

Figure 11: Microphone Setup for Acoustic test

Steady aerodynamics data

The **rake** (Figure 12) consists of 74 simple pitot tubes which are equally spaced by 3mm. The maximal measurement length is (74-1) x 3mm = 219mm . The number of measured probes is limited by available pressure ports on the pressure scanner. DLR used a 15 PSI module with 64 channels for data acquisition. This reduces the effective measurement length to (64-1) x 3mm = 189mm. The rake can be oriented either vertically or horizontally. For this measurement, it was oriented horizontally with respect to the model axis, i.e. parallel to the model's xy-plane. The rake was traversed either in the model's X- or Z-axis. A temperature sensor is located at probe position 26, (Y=1.5mm), but did not deliver useful data in combination with the data acquisition system.

The **data acquisition system** (DAQ, Figure 12) is a PressureSystems Netscanner Model 98RK which contains 3x16=48 ports and a PressureSystems Netscanner Model 9116 which contains 16 ports. The measurement range is 5 PSI (+20%) which corresponds to measuring a maximum jet Mach number Mjet<0.66. Each pressure channel is equipped with its own reference pressure. The reference of choice is the ambient pressure of the room/chamber.

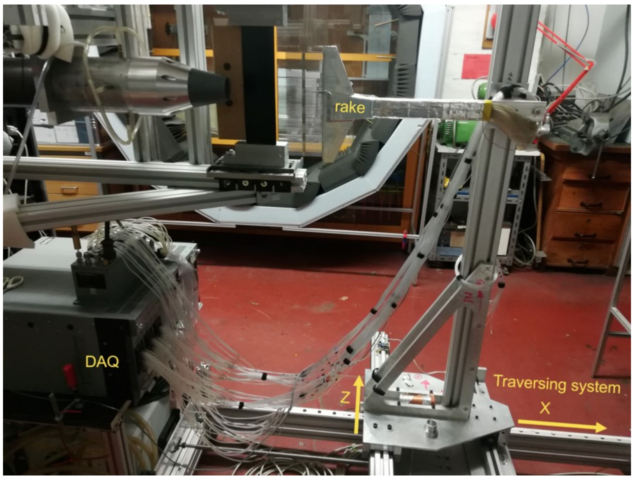

Figure 12: Rake setup for steady aerodynamics tests. The traversing system allows shifts along the model's X-axis and the model's Z-axis.

Hence dynamic pressures were acquired via a Labview module programmed by Johannes Stahn, stored in online data files and post-processed into Tecplot® readable data.

Three state properties are needed for a known position in order to derive the full set of mean flow properties, e.g. the measurement of total pressure p_t, static pressure p and total temperature T_t. The total pressure was measured with a set of i=1...64 simple pitot probes at each rake position j. Their spacing defines the resolution of the flow field (i,j). In addition, there are measurements which are not available for the full flow field (not individual for each probe i), but only 1 sample for each rake position j, i.e. 1 sample at a time:

- the total temperature (sourced from the test rig operations) and
- the ambient pressure (sourced from the test rig operations).

The assumption for static pressure distribution is equal static pressure across the flow field. This is in general a good assumption for a subsonic nozzle.

Total pressure at the rake

The simple pitot tubes measure the difference between the total pressure and the ambient pressure, i.e. the dynamic pressure Δp. Small negative difference pressure offsets cause errors in the data processing for compressible flow. They are corrected to the positive value of Δp(Δp<0)=0.1.

Static pressure

A correct static pressure measurement can detect any real expansion effects at the nozzle exit (e.g. $p = p_{amb}$ + 0...200 Pa) or static pressure deviations in the vicinity of curved surfaces, e.g. on the pressure side of the flap. However, this requires the use of pitot static tubes (https://en.wikipedia.org/wiki/Pitot_tube) (*German* name: Prandtl tubes (https://de.wikipedia.org/wiki/Pitotrohr)) which is not available in the test campaign. Instead, the subsonic engine outlet condition is used to estimate the ambient pressure of the entire flow field.

Total temperature

Since the total temperature of the JExTRA test rig T_t (j), is measured in the settling chamber of the air supply duct at very low velocity (< 1 m/s). Hence, high-speed corrections using the recovery factor (https://en.wikipedia.org/wiki/Total_air_temperature) are not necessary. The assumption is that adiabatic and reversible (i.e. isentropic) (https://en.wikipedia.org/wiki/Isentropic_process) flow conditions apply between settling chamber and rake and that the mixing between jet temperature and ambient room temperature is negligible.

Position

Nothing is as difficult as determining the real measurement position of the rake since the jet causes drag on the traversing system. Corrections of the position can be attempted by manual adjustment wrt. symmetric flow features. They require certainty about the symmetry.

Constants

The following constants were used for the calculation (Table 4):

Table 4: Constants

Property	Constant
Adiabatic index, cold air (https://en.wikipedia.org/wiki/Heat_capacity_ratio)	$\gamma = 1.40$
Specific gas constant, dry air (https://en.wikipedia.org/wiki/Gas_constant#Specific_gas_constant)	$R_{air} = 287.058 \frac{J}{kg\,K}$ [1] (https://de.wikipedia.org/wiki/Gaskonstante)

Calculated field properties

Once the field data for total temperature, ambient pressure and total pressure is defined, the following set of isentropic flow equations (https://www.grc.nasa.gov/WWW/K-12/airplane/isentrop.html) can be used to calculate related steady flow properties (Table 5):

Table 5: Calculated field properties

Property	Calculation
Pressure ratio (https://www.grc.nasa.gov/WWW/K-12/airplane/nozzleh.html)	$PR(i,j) := \frac{p_t}{p} = 1 + \frac{\Delta p(i,j)}{p_{AMB}(j)}$
Mach number (https://www.grc.nasa.gov/WWW/K-12/airplane/isentrop.html)	$M(i,j) = \sqrt{\frac{2}{\gamma-1} \cdot \left((PR(i,j))^{\frac{\gamma-1}{\gamma}} - 1 \right)}$
Static temperature (https://www.grc.nasa.gov/WWW/K-12/airplane/isentrop.html)	$T(i,j) = \frac{T_t(j)}{1 + \frac{\gamma-1}{2}(M(i,j))^2}$
Velocity (https://en.wikipedia.org/wiki/Mach_number)	$U(i,j) = M(i,j) \cdot \sqrt{\gamma R_{air} T(i,j)}$

Engine operations and test rig data

An operator typically enters a target Mach number or corresponding compressor RPM into the test rig's control panel, but how is it possible to know whether this input delivers the correct nozzle exit velocity? A rather strict, but perhaps scientifically correct measure was to challenge the correctness of the JExTRA test facility operation data. The jet nozzle exit velocity was recalculated (by the first-time users of the facility Christian Jente and Jean-Baptiste Mansoux) using only the available pressure and temperature measurements, internal rig geometry as well as fully compressible flow euqations of Isentropic flow (https://www.grc.nasa.gov/WWW/BGH/isentrop.html) (for duct contractions) as well Fanno flow (which accounts for wall friction in constant area ducts). The conventional results were found to be in very good agreement with the calculated results. This helped establish trust in the facility.

Contributed by: **Christian Jente, Henri Siller** — *DLR Deutsches Zentrum für Luft- und Raumfahrt*

Front Page	Introduction	Review of experimental studies	Description	Experimental Set Up	Measurement Quantities and Techniques	Data Quality and Accuracy	Measurement Data and Results

EXP 1-6 Data Quality and Accuracy

Mitigation of installed jet noise using porous flap trailing edges

Front Page	Introduction	Review of experimental studies	Description	Experimental Set Up	Measurement Quantities and Techniques	Data Quality and Accuracy	Measurement Data and Results

Data Quality and Accuracy of Measurements

Acoustics

- Long-term repeatability: The initial test was conducted in July 2021 and repeated in February 2022 (for the isolated jet noise only). The tests give the same results in the low- and mid-frequency range of the spectrum. Frequencies higher than 20kHz are strongly different, which stems from an improvement in the test setup. The test in July 2021 was conducted with installed protective microphone grids. The test team learned after the initial test that the very specific grid design limits the measurement to f<20kHz. Therefore, the second test was conducted without microphone protection grid. The results were used to correct the high-frequency data from the initial test.
- Accuracy of acoustic data when comparing to large-scale test facilities: The microphones are located at a distance of R_{cyl} = 573mm from the engine axis (R_{cyl}/D = 11.5). This does not satisfy the accepted distances ((R/D = 100)) for the geometric far-field of jet noise. Hence, a conventional comparison (i.e. assuming a negligible acoustic source dimension and all sources to be concentrated in the engine exit) to far-field jet noise from large scale tests is not possible. However, the cross-comparison is good when taking the distributed jet noise source into account (see data section and get uncertainty in [1] (https://elib.dlr.de/199634/)).

The lower frequency limit of ~500Hz has been determined by repeating the same measurement on a 1" nozzle using 1/4th and 1/8th inch microphones (Meyer, 2016 Penn State CAV Workshop). This corresponds to the compactness criterion for the source-observer distance, i.e. $f = \frac{340m/s}{0.573m} = 593Hz$.

Steady Aerodynamics (Rake)

Only the dynamic pressures of the pitot probe from the rake were measured for the entire field. The other properties were only determined at one position or underly assumptions. Hence, the accuracy of the physical field properties from high to low is:

- very high: measured dynamic pressures, i.e. total minus static
- high: total pressure and static pressure (assuming subsonic outlet conditions without any real expansion effects: <0.2%), as well as Mach number.
- mid: temperatures (not measured in the full field, only one global value) and velocities within the jet (local velocities are calculated with help of the Mach number and static temperature)
- low: temperatures and velocities within the test room (no test room temperature sensor installed)

The recommended velocity property for cross-comparison is the Mach number (see Figure 17 in the results section).

Contributed by: **Christian Jente, Henri Siller** — *DLR Deutsches Zentrum für Luft- und Raumfahrt*

Front Page	Introduction	Review of experimental studies	Description	Experimental Set Up	Measurement Quantities and Techniques	Data Quality and Accuracy	Measurement Data and Results

EXP 1-6 Measurement Data and Results

Mitigation of installed jet noise using porous flap trailing edges

Front Page | Introduction | Review of experimental studies | Description | Experimental Set Up | Measurement Quantities and Techniques | Data Quality and Accuracy | Measurement Data and Results

Measurement data/results

Geometry

The 3D CAD (https://en.wikipedia.org/wiki/Computer-aided_design) Geometry (Figure 14) is supplied as step file JExTRA_installed_jet_H30_L100.stp (https://kbwiki-data.s3-eu-west-2.amazonaws.com/EXP-1/6/CAD_Geometry/JExTRA_installed_jet_H30_L100.stp). The file includes microphone positions.

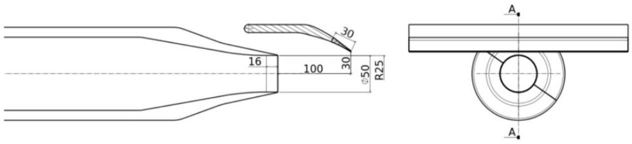

Figure 14: Scheme of installed engine

Acoustic data

A file named spmic_1295pn.tlt contains third-octave sound pressure level spectra for the microphones of test point 1295. The data has been calibrated, free-field incidence-corrected, atmosphere-corrected and R=1m distance-corrected w.r.t. the jet noise peak position. This information can be derived from the file name (Table 6), which is structured as *prefix_test-point_suffix.extension*.

Table 6: File name convention for acoustic data files

Prefix	**Type of spectrum**
spmic	Sound pressure level
psdmic	Power spectral density
0xxxx	**Test point number**
1295	installed jet vs. baseline flap
1375	installed jet vs. flap w/porous insert
1445	isolated jet
Suffix 1	**Measurement reference point (assumed source position)**
e	x=0, engine outlet
p	x=7D, assumed jet noise peak noise reference point
f	x=2D and z=0.6D, flap trailing edge
Suffix 2	**Use of tone removal tool**
n	no tone removal applied
b	tone removal, with the aim to extract the broadband effect alone. filter options listed in meta data. *Here*: Filtering w.r.t. median of each third-octave band with 50% overlap
Extension 1	**Signal versus background noise differences**
t	total, measured noise
c	total-background, corrected noise (*here* not applied)
Extension 2	**Instrumentation and acoustic laws**
u	uncorrected w.r.t instrumentation and acoustic laws
l	microphone incidence, loss-less atmosphere assuming a relative humidity of 0.50, distance corrected to R=1m w.r.t. assumed source point (see letter 4)
Extension 3	**Nature of the frequency bands**
n	narrowband frequency, *here resolved by* Δf=10Hz
t	third-octave band frequency resolution

The following data is available as csv (https://en.wikipedia.org/wiki/Comma-separated_values)-readable ASCII (https://en.wikipedia.org/wiki/ASCII)-files (Tables 7 to 9). They can be opened with any text editor or spreadsheet (https://en.wikipedia.org/wiki/Spreadsheet) editor: If microphones are placed far away from the sources, all noise sources can be assumed at the **engine exit**. The conventional assumption for the geometric far field is a microphone distance of 100 nozzle diameters towards the engine exit. The JExTRA microphones are positioned at a distance of merely 11.46 jet diameters towards the engine axis - much closer than the conventional geometric far field assumption requires. Yet, this data set of Table 7 is suited to evaluate the installation penalty and the noise reduction (Figure 15).

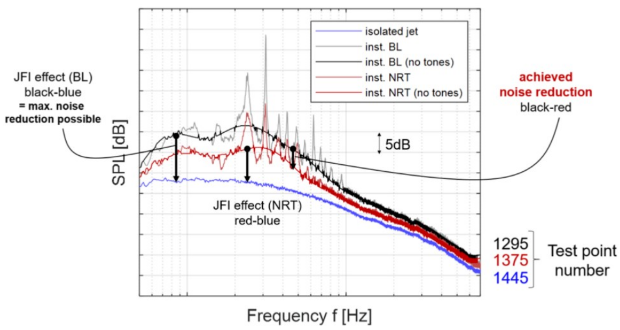

Figure 15: Installation effect and noise reduction: Spectra at Mic 1

The blue curve represents the isolated jet noise, i.e. without the wing being installed. The black curve represents the noise after installing the baseline wing. The black curve's shape consists of two humps at the low and mid frequency region as well as a broadband offset for the high frequency region. The cause of these acoustic effects are explained in the introduction.

The arithmetic difference between installed jet noise and isolated jet noise (black - blue) is the installation penalty (10dB in Figure 15). A perfect noise reduction technology would completely diminish the installation penalty. This is the reason why the baseline installation penalty is displayed in black on the left y-axis in Figure 16 c,d and e.

The installation noise of the porous NRT insert is displayed in red. While the knowledge of the absolute sound pressure level and new installation penalty (red - blue) is somewhat interesting, the more valuable information is how much better the porous NRT performs relative to the solid Baseline. Therefore, the difference between Baseline installation noise and NRT installation noise (black - red) is displayed in red on the right y-axis in Figure 16 c,d and e.

Apart from spectra at a single position, information on the directivity and jet Mach number behaviour is of interest. Spectral information SPL(f) can be summarized to the Overall Sound Pressure Level (OASPL) using logarithmic addition of the individual third-octave sound pressure levels. This helps to produce simple evaluations which are depicted in Figure 16 c,d and e.

The maximum installation effect occurs in the polar arc Figure 16 a and c, close to the overhead position (approximately perpendicular to the flap, Figure 16 b and d): For a jet Mach number of 0.6 (Figure 16e), the installation penalty is OASPL=10dB. With help of PA80-110, this penalty can be reduced by 5dB.

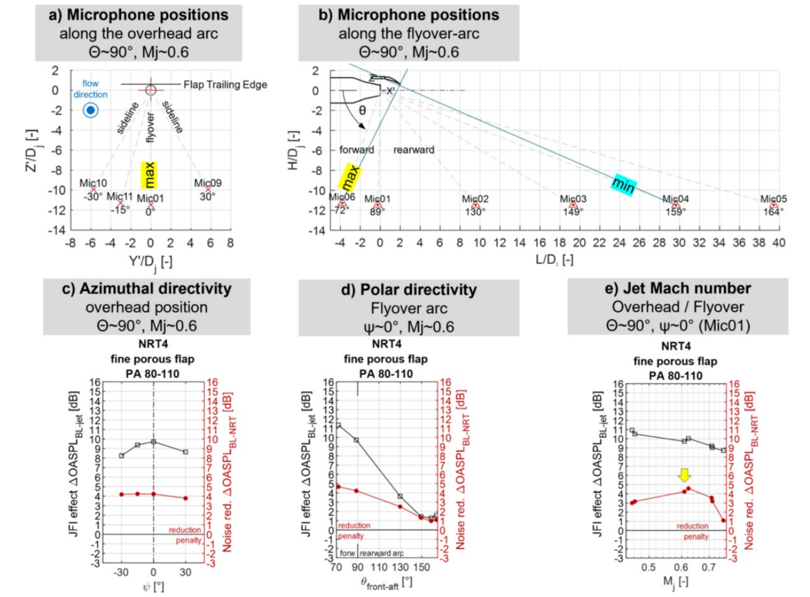

Figure 16: Comparison of acoustic installation effect (black) vs. achieved noise reduction (red) by azimuthal position (a and c) along the overhead arc, by polar directivity (b and d) along the flyover arc, and jet Mach number effect (e).

Table 7: Acoustic data, acoustic sources assumed at the engine exit

MRP=engine	1445 isolated	1295 installed	1375 installed NRT
SPL uncorrected	narrowband (https://kbwiki-data.s3-eu-west-2.amazonaws.com/EXP-1/6/Acoustics/dpt01445/spmic_1445en.tun)/third-oct (https://kbwiki-data.s3-eu-west-2.amazonaws.com/EXP-1/6/Acoustics/dpt01445/spmic_1445en.tut)	narrowband (https://kbwiki-data.s3-eu-west-2.amazonaws.com/EXP-1/6/Acoustics/dpt01295/spmic_1295en.tun)/third-oct (https://kbwiki-data.s3-eu-west-2.amazonaws.com/EXP-1/6/Acoustics/dpt01295/spmic_1295en.tut)	narrowband (https://kbwiki-data.s3-eu-west-2.amazonaws.com/EXP-1/6/Acoustics/dpt01375/spmic_1375en.tun)/third-oct (https://kbwiki-data.s3-eu-west-2.amazonaws.com/EXP-1/6/Acoustics/dpt01375/spmic_1375en.tut)
SPL corrected	narrowband (https://kbwiki-data.s3-eu-west-2.amazonaws.com/EXP-1/6/Acoustics/dpt01445/spmic_1445en.tln)/third-oct (https://kbwiki-data.s3-eu-west-2.amazonaws.com/EXP-1/6/Acoustics/dpt01445/spmic_1445en.tlt)	narrowband (https://kbwiki-data.s3-eu-west-2.amazonaws.com/EXP-1/6/Acoustics/dpt01295/spmic_1295en.tln)/third-oct (https://kbwiki-data.s3-eu-west-2.amazonaws.com/EXP-1/6/Acoustics/dpt01295/spmic_1295en.tlt)	narrowband (https://kbwiki-data.s3-eu-west-2.amazonaws.com/EXP-1/6/Acoustics/dpt01375/spmic_1375en.tln)/third-oct (https://kbwiki-data.s3-eu-west-2.amazonaws.com/EXP-1/6/Acoustics/dpt01375/spmic_1375en.tlt)
SPL tones removed	narrowband (https://kbwiki-data.s3-eu-west-2.amazonaws.com/EXP-1/6/Acoustics/dpt01445/spmic_1445eb.tln)/third-oct (https://kbwiki-data.s3-eu-west-2.amazonaws.com/EXP-1/6/Acoustics/dpt01445/spmic_1445eb.tlt)	narrowband (https://kbwiki-data.s3-eu-west-2.amazonaws.com/EXP-1/6/Acoustics/dpt01295/spmic_1295eb.tln)/third-oct (https://kbwiki-data.s3-eu-west-2.amazonaws.com/EXP-1/6/Acoustics/dpt01295/spmic_1295eb.tlt)	narrowband (https://kbwiki-data.s3-eu-west-2.amazonaws.com/EXP-1/6/Acoustics/dpt01375/spmic_1375eb.tln)/third-oct (https://kbwiki-data.s3-eu-west-2.amazonaws.com/EXP-1/6/Acoustics/dpt01375/spmic_1375eb.tlt)
PSD uncorrected	narrowband (https://kbwiki-data.s3-eu-west-2.amazonaws.com/EXP-1/6/Acoustics/dpt01445/psdmic_1445en.tun)/third-oct (https://kbwiki-data.s3-eu-west-2.amazonaws.com/EXP-1/6/Acoustics/dpt01445/psdmic_1445en.tut)	narrowband (https://kbwiki-data.s3-eu-west-2.amazonaws.com/EXP-1/6/Acoustics/dpt01295/psdmic_1295en.tun)/third-oct (https://kbwiki-data.s3-eu-west-2.amazonaws.com/EXP-1/6/Acoustics/dpt01295/psdmic_1295en.tut)	narrowband (https://kbwiki-data.s3-eu-west-2.amazonaws.com/EXP-1/6/Acoustics/dpt01375/psdmic_1375en.tun)/third-oct (https://kbwiki-data.s3-eu-west-2.amazonaws.com/EXP-1/6/Acoustics/dpt01375/psdmic_1375en.tut)
PSD corrected	narrowband (https://kbwiki-data.s3-eu-west-2.amazonaws.com/EXP-1/6/Acoustics/dpt01445/psdmic_1445en.tln)/third-oct (https://kbwiki-data.s3-eu-west-2.amazonaws.com/EXP-1/6/Acoustics/dpt01445/psdmic_1445en.tlt)	narrowband (https://kbwiki-data.s3-eu-west-2.amazonaws.com/EXP-1/6/Acoustics/dpt01295/psdmic_1295en.tln)/third-oct (https://kbwiki-data.s3-eu-west-2.amazonaws.com/EXP-1/6/Acoustics/dpt01295/psdmic_1295en.tlt)	narrowband (https://kbwiki-data.s3-eu-west-2.amazonaws.com/EXP-1/6/Acoustics/dpt01375/psdmic_1375en.tln)/third-oct (https://kbwiki-data.s3-eu-west-2.amazonaws.com/EXP-1/6/Acoustics/dpt01375/psdmic_1375en.tlt)
PSD tones removed	narrowband (https://kbwiki-data.s3-eu-west-2.amazonaws.com/EXP-1/6/Acoustics/dpt01445/psdmic_1445eb.tln)/third-oct (https://kbwiki-data.s3-eu-west-2.amazonaws.com/EXP-1/6/Acoustics/dpt01445/psdmic_1445eb.tlt)	narrowband (https://kbwiki-data.s3-eu-west-2.amazonaws.com/EXP-1/6/Acoustics/dpt01295/psdmic_1295eb.tln)/third-oct (https://kbwiki-data.s3-eu-west-2.amazonaws.com/EXP-1/6/Acoustics/dpt01295/psdmic_1295eb.tlt)	narrowband (https://kbwiki-data.s3-eu-west-2.amazonaws.com/EXP-1/6/Acoustics/dpt01375/psdmic_1375eb.tln)/third-oct (https://kbwiki-data.s3-eu-west-2.amazonaws.com/EXP-1/6/Acoustics/dpt01375/psdmic_1375eb.tlt)

Since the geometric far-field condition is not fulfilled for this test, comparison to other experiments are better, if specific source points are taken into account: For the evaluation of installation noise, all noise sources are assumed at the **flap trailing edge** (Table 8). For a fair cross-comparison to other facilities, tones are removed.

Table 8: Acoustic data, acoustic sources assumed at the flap trailing edge

MRP=flap	1445 isolated	1295 installed	1375 installed NRT
SPL uncorrected	-	-	-
SPL corrected	-	narrowband (https://kbwiki-data.s3-eu-west-2.amazonaws.com/EXP-1/6/Acoustics/dpt01295/spmic_1295fn.tln)/third-oct (https://kbwiki-data.s3-eu-west-2.amazonaws.com/EXP-1/6/Acoustics/dpt01295/spmic_1295fn.tlt)	narrowband (https://kbwiki-data.s3-eu-west-2.amazonaws.com/EXP-1/6/Acoustics/dpt01375/spmic_1375fn.tln)/third-oct (https://kbwiki-data.s3-eu-west-2.amazonaws.com/EXP-1/6/Acoustics/dpt01375/spmic_1375fn.tlt)
SPL tones removed	-	narrowband (https://kbwiki-data.s3-eu-west-2.amazonaws.com/EXP-1/6/Acoustics/dpt01295/spmic_1295fb.tln)/third-oct (https://kbwiki-data.s3-eu-west-2.amazonaws.com/EXP-1/6/Acoustics/dpt01295/spmic_1295fb.tlt)	narrowband (https://kbwiki-data.s3-eu-west-2.amazonaws.com/EXP-1/6/Acoustics/dpt01375/spmic_1375fb.tln)/third-oct (https://kbwiki-data.s3-eu-west-2.amazonaws.com/EXP-1/6/Acoustics/dpt01375/spmic_1375fb.tlt)
PSD uncorrected	-	-	-
PSD corrected	-	narrowband (https://kbwiki-data.s3-eu-west-2.amazonaws.com/EXP-1/6/Acoustics/dpt01295/psdmic_1295fn.tln)/third-oct (https://kbwiki-data.s3-eu-west-2.amazonaws.com/EXP-1/6/Acoustics/dpt01295/psdmic_1295fn.tlt)	narrowband (https://kbwiki-data.s3-eu-west-2.amazonaws.com/EXP-1/6/Acoustics/dpt01375/psdmic_1375fn.tln)/third-oct (https://kbwiki-data.s3-eu-west-2.amazonaws.com/EXP-1/6/Acoustics/dpt01375/psdmic_1375fn.tlt)
PSD tones removed	-	narrowband (https://kbwiki-data.s3-eu-west-2.amazonaws.com/EXP-1/6/Acoustics/dpt01295/psdmic_1295fb.tln)/third-oct (https://kbwiki-data.s3-eu-west-2.amazonaws.com/EXP-1/6/Acoustics/dpt01295/psdmic_1295fb.tlt)	narrowband (https://kbwiki-data.s3-eu-west-2.amazonaws.com/EXP-1/6/Acoustics/dpt01375/psdmic_1375fb.tln)/third-oct (https://kbwiki-data.s3-eu-west-2.amazonaws.com/EXP-1/6/Acoustics/dpt01375/psdmic_1375fb.tlt)

For the cross-comparison of isolated jet noise, all noise sources are assumed to origin at the engine axis 7 jet diameters downstream the engine exit (Table 9). This should give good low frequency comparability to other jet noise data. [1] (https://elib.dlr.de/199634/) The nature of a distributed jet noise source is ignored. This leads to some error, since higher frequencies are closer located to the engine exit.

Table 9: Acoustic data, acoustic sources assumed 7 jet diameters downstream the engine exit

MRP=low freq. peak	1445 isolated	1295 installed	1375 installed NRT
SPL uncorrected	-	-	-
SPL corrected	narrowband (https://kbwiki-data.s3-eu-west-2.amazonaws.com/EXP-1/6/Acoustics/dpt01445/spmic_1445pn.tln)/third-oct (https://kbwiki-data.s3-eu-west-2.amazonaws.com/EXP-1/6/Acoustics/dpt01445/spmic_1445pn.tlt)	-	-
SPL tones removed	narrowband (https://kbwiki-data.s3-eu-west-2.amazonaws.com/EXP-1/6/Acoustics/dpt01445/spmic_1445pb.tln)/third-oct (https://kbwiki-data.s3-eu-west-2.amazonaws.com/EXP-1/6/Acoustics/dpt01445/spmic_1445pb.tlt)	-	-
PSD uncorrected	-	-	-
PSD corrected	narrowband (https://kbwiki-data.s3-eu-west-2.amazonaws.com/EXP-1/6/Acoustics/dpt01445/psdmic_1445pn.tln)/third-oct (https://kbwiki-data.s3-eu-west-2.amazonaws.com/EXP-1/6/Acoustics/dpt01445/psdmic_1445pn.tlt)	-	-
PSD tones removed	narrowband (https://kbwiki-data.s3-eu-west-2.amazonaws.com/EXP-1/6/Acoustics/dpt01445/psdmic_1445pb.tln)/third-oct (https://kbwiki-data.s3-eu-west-2.amazonaws.com/EXP-1/6/Acoustics/dpt01445/psdmic_1445pb.tlt)	-	-

Steady aerodynamic data

The measurement planes (Figure 17) are available as Tecplot (https://en.wikipedia.org/wiki/Tecplot)-readable ASCII (https://en.wikipedia.org/wiki/ASCII)-files in Table 10.

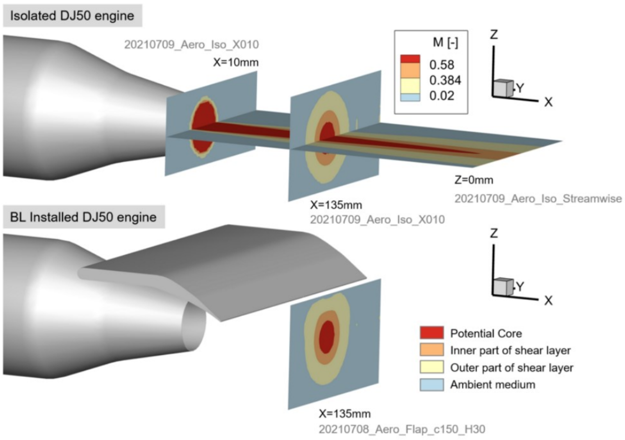

Figure 17: Overview of steady aerodynamics data, showing Mach number contours at the horizontal plane at Z=0 and at a cross-sectional plane at X=135mm

Table 10: Steady aerodynamics data, by plane

File	X [mm]	Y [mm] (rake)	Z [mm]
20210709_Aero_Iso_Streamwise.dat (https://kbwiki-data.s3-eu-west-2.amazonaws.com/EXP-1/6/Aero/20210709_Aero_Iso_Streamwise.dat)	[10 20 30 40 60 80 120 160 240 320]	[-78:3:108]	0
20210709_Aero_Iso_X010.dat (https://kbwiki-data.s3-eu-west-2.amazonaws.com/EXP-1/6/Aero/20210709_Aero_Iso_X010.dat)	10	[-78:3:108]	[36:-3:-36]
20210709_Aero_Iso_X135.dat (https://kbwiki-data.s3-eu-west-2.amazonaws.com/EXP-1/6/Aero/20210709_Aero_Iso_X135.dat)	135	[-78:3:108]	[48:-3:-48]
20210708_Aero_Flap_c150_H30.dat (https://kbwiki-data.s3-eu-west-2.amazonaws.com/EXP-1/6/Aero/20210708_Aero_Flap_c150_H30.dat)	135	[-78:3:108]	[39:-3:-57]

The X=135mm plane displays the difference between the symmetric isolated jet and the deformed installed jet. The data allows to extract some general properties of the aerodynamic near field jet shear layer, e.g. half-jet opening angle, virtual shear layer origin and effective jet diameter (Figure 18). Besides this, the data serves mainly for numerical cross-comparison.

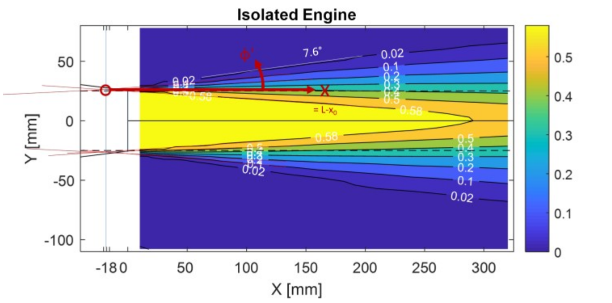

Figure 18: Evaluation of steady aerodynamics data in plane Z=0mm, revealing the half-jet opening angle of 7.5° and the virtual origin of the near field jet shear layer at x0=-18mm

However, the steady aerodynamics data allows for some general conclusions about the flow type and the expected acoustic spectrum in the high-, mid- and low-frequency region:

- The rather undisturbed circular jet potential core (red in Figure 17) and inner shear layer (orange in Figure 17) tells that there is no significant high-frequency installation penalty. The deviation from the isolated jet noise is smaller than the value for reflections on the unshielded side, i.e. 3dB.
- The deformed outer shear layer is - only in this type of experiment - an indicator for jet-flap interaction. It indicates a large mid-frequency installation penalty.
- The low-frequency installation penalty cannot be estimated from the steady aerodynamics flow field, but a first estimate can be made based on the installation geometry in terms of the vertical proximity H and the curvature of the wing.

Contributed by: **Christian Jente, Henri Siller** — *DLR Deutsches Zentrum für Luft- und Raumfahrt*